**Article:**

Raveendran, R, Nagaraj, M orcid.org/0000-0001-9713-1362 and Namboothiry, MAG (2020) High performance, transparent solution-processed organic field effect transistor with low-k elastomeric gate dielectric and liquid crystalline semiconductor: Promises and Challenges. ACS Applied Electronic Materials. acsaelm.0c00635. ISSN 2637-6113

https://doi.org/10.1021/acsaelm.0c00635

ACS APPLIED ELECTRONIC MATERIALS



Article

# High performance, transparent solution-processed organic field effect transistor with low-k elastomeric gate dielectric and liquid crystalline semiconductor: Promises and Challenges

Reshma Raveendran, Mamatha Nagaraj, and Manoj A G Namboothiry

*ACS Appl. Electron. Mater.*, **Just Accepted Manuscript** • DOI: 10.1021/acsaelm.0c00635 • Publication Date (Web): 13 Sep 2020

# High performance, transparent solution-processed organic field effect transistor with low-k elastomeric gate dielectric and liquid crystalline semiconductor: Promises and Challenges

*Reshma Raveendran[1], Mamatha Nagaraj[2] and Manoj A. G. Namboothiry[1],**

[1]School of Physics, Indian Institute of Science Education and Research- Thiruvananthapuram, Maruthamala P O, Vithura, Thiruvananthapuram, Kerala- 695551, India

E-mail: manoj@iisertvm.ac.in

[2]School of Physics and Astronomy, University of Leeds, Leeds LS2 9JT, UK

E-mail: m.nagaraj@leeds.ac.uk

**KEYWORDS:** organic field effect transistors, elastomers, polydimethylsiloxane, liquid crystals, mobility, transparent, double-slope, anomalous bias-stress

**ABSTRACT:** The highly flexible and stretchable polymer elastomer having a low dielectric constant (k~ 2.6), called poly(dimethylsiloxane) (PDMS), is a promising gate dielectric material for solution-processed organic field effect transistors (OFETs). A detailed understanding of PDMS based OFETs is required to extend its application to flexible electronic devices. The present work discusses about the promises and challenges of PDMS based solution-processed OFETs using a liquid crystal (LC), 2-decyl-7-phenyl-benzothienobenzothiophene (Ph-BTBT-10) as semiconducting channel material. The liquid crystal-OFET (LC-OFET) exhibits high electrical performance such as high hole mobility of ~ 22 $cm^2V^{-1}s^{-1}$, low threshold voltage (< 1 V) and high current on/ off ratio of $10^5$. The OFETs also show high optical transparency (> 90 %). The electrical performance of LC-OFETs are observed to have a significant correlation with the annealing temperature of Ph-BTBT-10 layer and is also influenced by the different operating conditions such as air, nitrogen and vacuum. The OFETs demonstrate anomalous bias stress behavior and hysteresis which are also addressed.

## INTRODUCTION

Organic field effect transistor (OFET), a vital key component in organic electronic circuits, is actively investigated during the last thirty years and tremendous progress has been made in its performance. OFETs have the potential to enable large area, flexible electronic circuitry at a low-cost of production and find application in radio frequency identification (RFID) tags, smart cards, electronic papers and active matrix displays.[1] Moreover, OFETs with high optical transparency and environmental stability are potentially suitable for next generation transparent electronics such as flat panel displays and sensor arrays.[2-5] The unique features of mechanical flexibility, tunability of electrical and optical properties and solution-processability enjoyed by OFETs are realized by the organic components used in them, namely the organic semiconductor (OSC), the gate dielectric and the electrodes.[6-8]

Gate dielectric plays a crucial role in determining the characteristics of an OFET as the channel is just a few monolayers above the dielectric.[7, 9-12] In most of the high-performance OFETs reported so far, the conventional inorganic materials such as silicon dioxide ($SiO_2$), aluminum oxide ($Al_2O_3$) and so on are used as gate dielectrics along with solution-processed OSCs.[13-20] Though, all-solution-processed OFETs are essential for the realization of low-cost, flexible electronic devices, the development of such OFETs in which both the gate dielectric and the semiconductor are organic materials is difficult to achieve. The reason being the difficulty in forming pin-hole free dielectric thin-films with controlled morphology and selection of suitable orthogonal solvent for both the semiconductor and the gate dielectric.[12] However, there is a large improvement in the development of flexible gate dielectrics these days.[8, 21-25] To ensure good electrical performance, dielectrics of high dielectric constant (high-k) are often suggested.[26] However, as high-k materials suffer from large dipole disorder, high gate leakage current, large power dissipation and low reproducibility, low-k dielectrics can be considered to make more reliable low-power devices.[7-8, 10, 21, 27-29] Among the various low-k dielectrics, the polymer elastomer, polydimethylsiloxane (PDMS), is a promising candidate as a gate dielectric in OFETs as it exhibits high flexibility, stretchability and good optical transparency.[30-33] However, it has mainly been used along with vacuum-deposited semiconductors, as solution-processing on PDMS surface is difficult due to its high hydrophobic nature and low surface energy.[33-35] The applicability of PDMS in OFETs is critically limited by these aspects and hence it is less explored. Our recent work has shown that the wettability and adhesion of organic solutions on PDMS can be accomplished by mere treatment of PDMS surface with ultra-violet ozone (UVO) for an extended period of time. Our findings demonstrated the possibility of using PDMS as a gate dielectric in all-solution-processed OFETs.[36]

The applicability of OFETs in electronic circuits is assessed by its current on-off ratio and switching frequency.[37] Since both these parameters are highly dependent on charge carrier mobility, it remains a crucial figure of merit of OFETs.[37-38] Significant efforts have been devoted to realize high mobility OSCs which form the channel for carrier conduction in FETs. OFETs fabricated with solution-processed OSCs are reported to show field effect mobilities above 10 $cm^2V^{-1}s^{-1}$.[2, 13-20, 39] Crystallinity and uniformity of the semiconducting films critically affect the mobility. In most of the solution-processed films, poor uniformity and high roughness occur due to recrystallization of the materials during solvent evaporation.[9] In this perspective, there is much focus on the utilization of solution-processable semiconducting liquid crystals (LCs) that form high-quality dielectric-semiconductor interfaces by enhanced crystalline ordering and self-alignment, thereby improving the charge carrier transport through the channel.[13, 40-41] Besides this, the temperature stability of LCs from ambient to 100-200 $^0$C promises viable practical applications.[41] In this work, we address these issues and report OFETs of high mobilities, fabricated on flexible polymer elastomer called PDMS.

Recently, Iino and coworkers developed a LC semiconducting material namely, 2-decyl-7-phenyl-benzothienobenzothiophene (Ph- BTBT-10) which shows two LC mesophases, smectic E (SmE) and smectic A (SmA). They demonstrated the application of Ph-BTBT-10 as channel material in OFETs with the conventional gate dielectric, silicon dioxide ($SiO_2$) and the OFETs exhibited a mobility value of 13.9 $cm^2V^{-1}s^{-1}$.[9] The high mobility is attributed to the closely packed crystal-like molecular ordering (called herringbone structure) of Ph-BTBT-10 in its SmE phase which allows two-dimensional conduction.[9] The same group has investigated the characteristics of Ph-BTBT-10 based OFET with a hybrid gate insulator, polystyrene (PS)/ $SiO_2$ and obtained a low average threshold voltage ($V_{th}$) of - 0.12 ± 0.09 V, compromising the mobility ($\mu_{sat}$= 3.8 ±

0.27 $cm^2V^{-1}s^{-1}$) and flexibility.[10] Later, Kim et al. studied the effect of semiconductor annealing temperatures on the performance of OFETs fabricated with polyimide (PI)/ alumina ($Al_2O_3$) gate dielectric. They obtained a maximum mobility of 2.27 $cm^2V^{-1}s^{-1}$ with Ph-BTBT-10 layer annealed at 140 $^0$C (temperature corresponds to the SmE phase) but the devices operated at a high $V_{th}$ of ~ - 12 V.[11] In all these reports, either a conventional gate dielectric ($SiO_2$) or a bilayer of organic and conventional gate dielectric (PS/ $SiO_2$ and PI/ $Al_2O_3$) are used. Implementation of elastomeric gate dielectrics in LC-OFETs is less reported in the literature and since each dielectric-semiconductor interface has its unique features, it would be interesting to investigate how an elastomeric gate dielectric such as PDMS influences the performance of LC-OFETs. Being a well-known material for its high flexibility and stretchability, the incorporation of PDMS in OFETs may have a future implication in the development of flexible electronic devices.

In the present work, the performance of solution-processed OFETs with Ph-BTBT-10 as semiconductor and PDMS as gate dielectric is discussed. Two sets of OFETs have been fabricated for the studies, one set is made in ambient air and the other set is fabricated in inert condition (in nitrogen atmosphere). Surface treated PDMS layer (extended ultra violet-ozone (UVO) treatment for 60 minutes) is used in the study. A detailed description of UVO treatment and its consequences are described in our previous work.[36] A systematic study on the effect of different annealing temperatures of Ph-BTBT-10 layer on the performance of OFETs is conducted and the effect of different environmental conditions is evaluated. Deviation from ideal transistor behavior is observed in the OFETs in the form of double slopes which can cause overestimation of the mobility values.[42] This issue has been addressed and the reliability of extracted mobilities is inspected by calculating 'reliability factor (r)' as recently reported by H. H. Choi et al.[42] Accordingly, the OFET with Ph-BTBT-10 layer annealed at 120 $^0$C in air exhibited the highest mobility of ~ 22.7 $cm^2$ $V^{-1}$

$s^{-1}$, low threshold voltage (+ 0.76 V) and high current on/ off ratio ($10^5$) compared to other OFETs. The LC-OFET also exhibited good transparency (> 90%) owing to the transparent nature of the components, indium tin oxide (ITO) gate electrode, PDMS and Ph-BTBT-10 used in the device architecture. The correlation between the outstanding performance of OFETs with the change in morphology and crystallinity of Ph-BTBT-10 with annealing temperature is investigated. The crystalline and morphological features of annealed films of Ph-BTBT-10 are studied by means of small angle x-ray scattering (SAXS), x-ray diffraction (XRD) and atomic force microscopy (AFM) techniques. The electrical stability of OFETs is analyzed by conducting bias-stress measurements and the environmental stability is analyzed by evaluating the OFET performance in air, nitrogen and vacuum conditions. Hysteresis is observed in the PDMS based LC-OFETs which is also discussed in detail.

## EXPERIMENTAL SECTION

***Materials.*** Commercially available Ph-BTBT-10 (MW= 456.706 g/mol) from TCI Chemicals and PDMS along with its curing agent (Sylgard 184) from Dow corning were used as the semiconductor and gate dielectric respectively. ITO substrates were purchased from (10 $\Omega/cm^2$) Delta Technologies Inc., USA.

***LC-OFET fabrication.*** The OFETs were fabricated in the bottom-gate top-contact (BGTC) configuration (figure 1a) on ITO coated glass substrates. The gate dielectric, PDMS and the semiconductor, Ph-BTBT-10 (chemical structures as shown in figure 1b) were solution-processed using spin-coating method. PDMS was mixed thoroughly with a curing agent at 10:1 w/w ratio to initiate cross-linking and mixed with cyclohexane (PDMS/ cyclohexane= 1:6 w/w ratio) to reduce the viscosity of the solution. Thin-films of PDMS was prepared by spin-coating PDMS solution at an rpm of 6000 on ITO substrate and annealed the layer at 150 $^0$C for 30 minutes. These films with thickness around 1.2 μm (measured using Alpha-Step D-600 Stylus Profiler, KLA Tencor) were UVO treated for 60 minutes in a UV-Ozone cleaner with an output power of 9 mW/cm$^2$ (UVOCS, USA) to enhance the surface wettability of PDMS (more details on the UVO treatment of PDMS surface is provided in the supporting information). Thin- films of Ph-BTBT-10 was spin-coated from a solution prepared by dissolving it in chlorobenzene (CB) (0.66 wt %). Prior to spin-coating, the solution was stirred by heating it at 160 $^0$C for 5 minutes and kept for continuous stirring at 110 $^0$C to ensure complete dissolution. At this temperature, the LC exists in one of its mesophases called, the SmE phase (details of the polarization optical microscopy (POM) and differential scanning calorimetry (DSC) studies of the LC are given in the supplementary data, figure S1). The solution was immediately spin-coated on PDMS surface to avoid sudden crystallization into bulk layers. The layers were annealed at different temperatures (120 $^0$C, 180 $^0$C and 218 $^0$C) for 10 minutes each. The Ph-BTBT-10 film thickness was measured to be ~ 35 nm. The source and drain electrodes were deposited by the thermal evaporation of gold (Au) using a mask with channel length, L= 30 μm and channel width, W= 1 mm.

***LC-OFET characterization.*** The OFETs were characterized using Keithley SCS 4200 Parameter analyzer and the mobility in the saturation regime ($\mu_{sat}$) was calculated using the following equation,

$$\mu_{sat} = \frac{2L}{W\,C_i}\left(\frac{\partial\sqrt{I_{DS}}}{\partial V_{GS}}\right)^2 \qquad (1)$$

Where $C_i$ is the capacitance per unit area of the gate dielectric, $W$ is the channel width and $L$ is the channel length. The capacitance characterization of PDMS is conducted using Agilent E4980A Precision LCR Meter.

The reliability of the extracted mobilities are examined by calculating 'reliability factor (r)' as suggested by Choi *et al*., using the equation given below.

The reliability factor (r) in the saturation regime:[42]

$$r_{sat} = \left(\frac{\sqrt{|I_{DS}|_{max}} - \sqrt{|I_{DS}|_{0}}}{|V_{GS}|_{max}}\right)^2 / \left(\frac{\partial\sqrt{|I_{DS}|}}{\partial V_{GS}}\right)^2_{claimed} \quad (2)$$

where, $|I_{DS}|_{max}$ is the maximum saturation drain current for the maximum gate to source voltage ($|V_{GS}|_{max}$), $|I_{DS}|_0$ is the drain current at zero $V_{GS}$, $\mu_{claimed}$ is the claimed mobility obtained directly from the Shockley equation (1). The experiments were conducted in air, nitrogen and vacuum conditions.

***Characterization of Ph-BTBT-10.*** To study the characteristics of Ph-BTBT-10, the polarization optical microscopy (POM) images were taken using Leica DM2700P polarization microscope. The sample was mounted on a Linkam THMS600 hot stage and the temperature was controlled using Linkam T95-PE temperature controller (cooling rate 0.1 $^0$C/min). Differential scanning calorimetry (DSC) measurements were done using DSC Q20, TA Instruments. Small angle X-ray scattering (SAXS) was done using Xeuss SAXS/WAXS system, Xenocs. The crystalline properties and morphology of the LC films on glass substrate and on PDMS surface were studied using X-ray diffraction (PANalytical Empyrean XRD) and atomic force microscopy (Nanowizard 4 AFM, JPK Instruments) techniques respectively. The transparency of Ph-BTBT-10 films were evaluated using an ultraviolet-visible spectroscopic technique (LAMBDA 950 UV/Vis Spectrophotometer, PerkinElmer). Bias- stress measurements were conducted by using two source meters from Keithley (6430 and 2400).

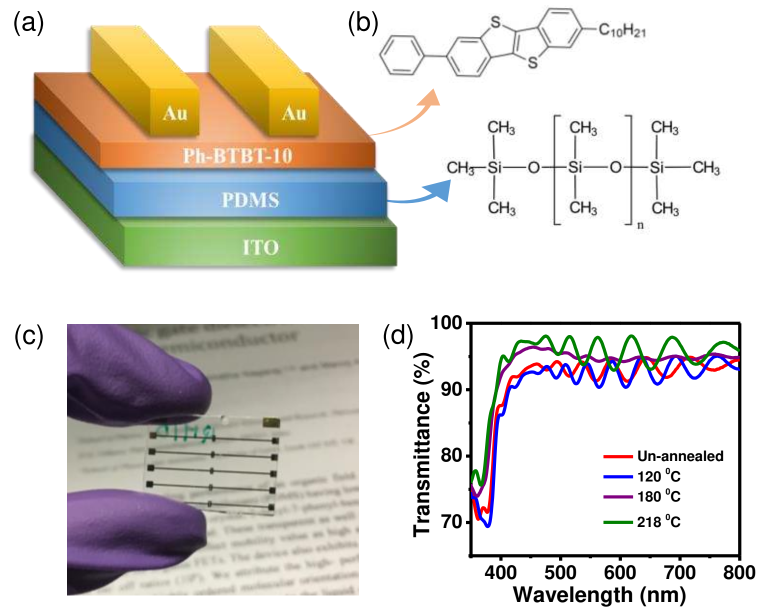


**Figure 1.** (a) Schematic representation of the device architecture of a bottom-gate top-contact OFET. (b) Molecular structure of the liquid crystal, Ph-BTBT-10 (top) and the polymer, PDMS (bottom). (c) Photograph showing a prepared transparent OFET and (d) UV-Visible transmission spectra of ITO/ PDMS/ Ph-BTBT-10 film structure at different annealing temperatures of Ph-BTBT-10.

## RESULTS AND DISCUSSION

**Transistor Characteristics at different annealing temperatures of Ph-BTBT-10.** The solution-processed OFETs are fabricated in the bottom-gate top-contact (BGTC) configuration using PDMS as gate dielectric and Ph-BTBT-10 as semiconductor material (Figure 1a, 1b). Solution-processing of Ph-BTBT-10 is enabled on PDMS surface by extended ultra violet-ozone (UVO) treatment as discussed in our previous work.[36] The UVO working mechanism is included in the supporting information. The gate dielectric PDMS of thickness around 1.2 µm exhibits a capacitance per unit area ($C_i$) of ~ 1.92 nF $cm^{-2}$ at frequency, f= 1 kHz. The capacitance-frequency plot of PDMS (figure S2) shows almost a constant value of capacitance for a long range of frequency (100 Hz to 2 MHz). The semiconductor, Ph-BTBT-10 formed uniform thin layer of thickness ~ 35 nm which is annealed at different temperatures, 120 $^0$C, 180 $^0$C and 218 $^0$C, to analyze its effect on the electrical performance of LC-OFETs. The temperatures were chosen in such a way that the LC exists in the SmE phase (at 120 and 180 $^0$C) and in the SmA phase (at 218 $^0$C) during annealing (figure S1). Figure 1c shows the photograph of the prepared LC-OFET. The OFETs at all annealing temperatures exhibit high optical transparency > 90 % in the visible region as shown in the UV-vis transmission spectra (figure 1d). More than twenty devices have been fabricated at each annealing temperatures by keeping other processing conditions the same and the best characteristics obtained are shown in figure 2. The devices exhibited small gate leakage currents which are 2-3 orders lower than the drain current as seen in figure 2(b,d,f and h). The output characteristics of all the devices showed distinct linear and saturation regimes with drain current ($I_{DS}$) in the mA range for different applied gate voltages ($V_{GS}$). However, the output characteristics exhibited non-linear behavior at low drain to source voltage ($V_{DS}$) which indicates the presence of substantial contact resistance.[43-44] The main source of contact resistance is the misalignment between the work function of gold electrode (- 5.1 eV) and the highest occupied molecular orbital (HOMO) energy level of Ph-BTBT-10 (- 5.6 eV).[43, 45] A non-ideal behavior is observed in the transfer characteristics of OFETs in the form of double slopes (or kinks) where the Ph-BTBT-10 film is either un-annealed or annealed at 120 $^0$C (figure 2b and 2d). Kink in the transfer characteristics are often caused by contact effects in OFETs.[44, 46] Here, the appearance of kinks in OFETs with the semiconductor film annealed at certain specific temperatures indicates its correlation with the changes occurring in the microstructure of the film or at the semiconductor-dielectric interface. As it is seen in the figures 2b and 2d, there are two slopes in the transfer curve (a high slope region at low $V_{GS}$ and a small slope region at high $V_{GS}$). Therefore, the conventional way of calculation can lead to wrong estimation of mobilities.[42, 44] Being a common issue among high mobility OFETs,[2, 47] it is often suggested to estimate the mobility from low slope (high $V_{GS}$) region of the transfer curve in order to get more accurate value.[42, 44, 48] We have calculated mobilities using both the slopes and analyzed the closeness of the derived mobilities (for the OFETs with double-slope) to an equivalent OFET with the same maximum saturation current ($I_{D\ sat}$) at a maximum gate voltage ($V_{GS}$) using reliability factor (r) calculation (equation 2 in the experimental section) which is recently suggested by H. H. Choi et al (summarized in table S1).[42] The mobilities derived from the high slope region of OFETs with Ph-BTBT-10 film un-annealed and annealed at 120 $^0$C are found to have low reliability factors (43 and 34 % respectively) compared to that of the equivalent ideal OFET. Whereas, the mobilities derived from the small slope region are found to be closer to the mobility of equivalent OFETs with reliability factors 92 and 91 % respectively. Hence, we choose the mobility derived from the small slope region as the original hole mobility for those devices which show the abnormal 'kinks'. The threshold voltages $V_{th}$ are also obtained by considering the small slope in the $\sqrt{I_{DS}}$ vs $V_{GS}$ curve. The mobility of the devices annealed at 180 and 218 $^0$C are obtained using the conventional method. Linear mobility of the OFETs are not included in the table as they are prone to contact effects. The electrical parameters obtained for the OFETs shown in figure 2 are as given in table 1. The average mobilities of ten to fifteen OFETs for each annealing temperatures are tabulated (table S2) and the variation in mobility with different annealing temperatures of Ph-BTBT-10 are shown in figure S3 (the figure also shows the mobility values of the devices annealed at intermediate temperatures of 100 and 150 $^0$C with error bars included) where sudden jump in mobility at 120 $^0$C is clearly visible. A similar trend is observed in the case of threshold voltages and current on/ off ratios also. It is to be noted that some of the OFETs showed mobilities higher than the highest value reported here, but were not reproducible and therefore avoided.

It is seen that the transistor characteristics show significant dependence on the annealing temperatures (un-annealed, annealed at 120 $^0$C, 180 $^0$C and 218 $^0$C) of Ph-BTBT-10 film. Among them, the OFET with LC film annealed at 120 $^0$C exhibited considerably higher drain currents, high mobility, low threshold voltage and high current on-off ratio compared to other OFETs. The hole- mobility of the OFET with un-annealed Ph-BTBT-10 layer is obtained as 5.56 cm$^2$ V$^{-1}$ s$^{-1}$ and possessed a low $V_{th}$ of – 0.87 V, when calculated from the low-slope (high $V_{GS}$ region). As the annealing temperature is increased to 120 $^0$C, the mobility increased almost four times to 22.71 cm$^2$ V$^{-1}$ s$^{-1}$, which is to the best of our knowledge, the highest mobility value reported for Ph-BTBT-10 based OFET. The mobility averaged for twenty devices are obtained as 22 ± 2 cm$^2$ V$^{-1}$ s$^{-1}$. The device is operated at a very low, close to zero $V_{th}$ of + 0.76 V and exhibited high current on/ off ratio of ~ 10$^5$. However, for the OFET with Ph-BTBT-10 layer annealed at 180 $^0$C, the mobility fall down to 3.41 cm$^2$ V$^{-1}$ s$^{-1}$ and the $V_{th}$ is increased to -12.06 V. On further increasing the annealing temperature to 218 $^0$C, a sudden drop in mobility to 0.5 cm$^2$ V$^{-1}$ s$^{-1}$ along with a rise in $V_{th}$ is observed.

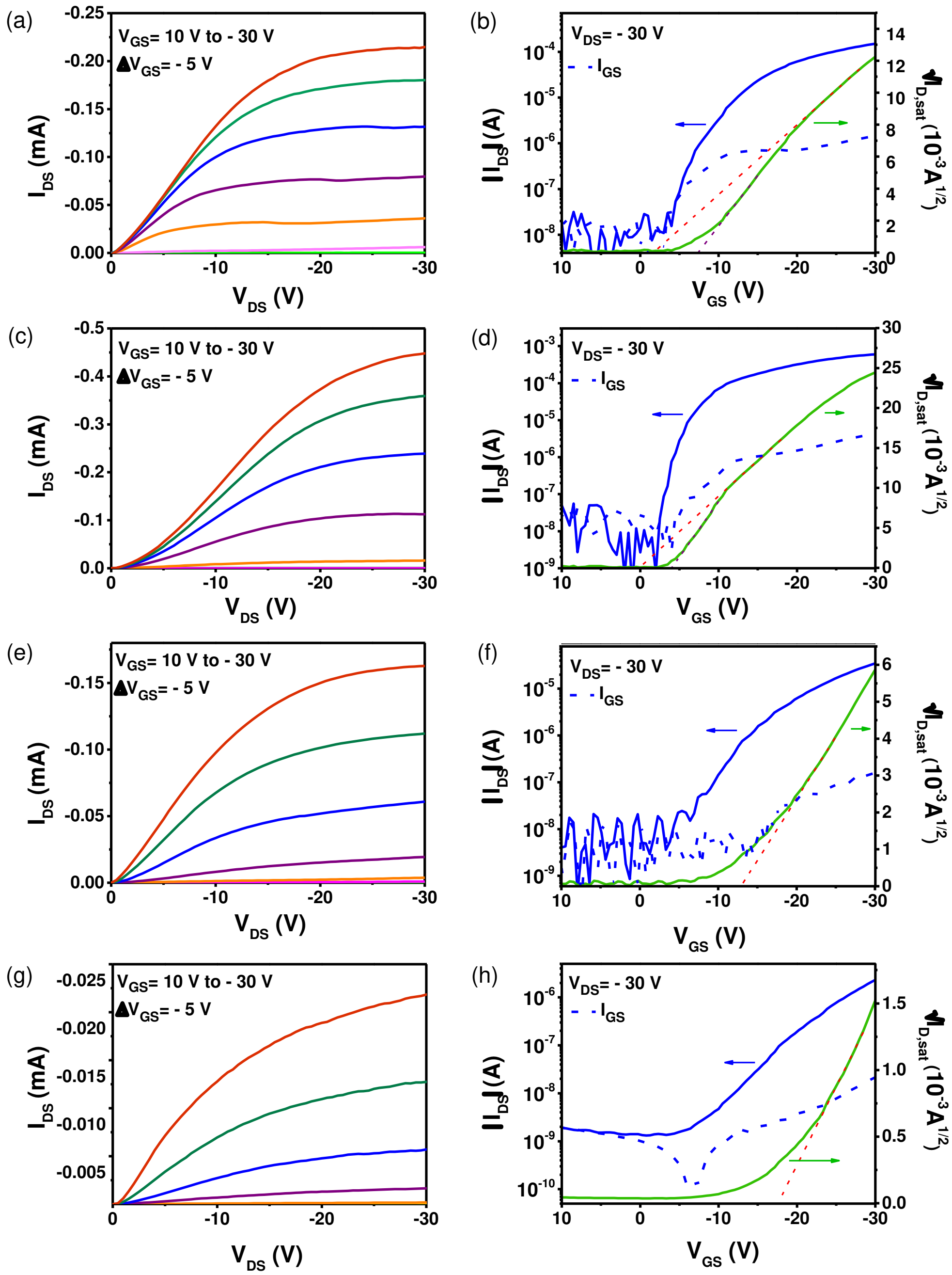


**Figure 2.** (a, c, e, g) Output characteristics ($I_{DS}$ -$V_{DS}$) and (b, d, f, h) transfer characteristics ($|I_{DS}|$-$V_{GS}$ and $\sqrt{I_{D, sat}}$ -$V_{GS}$) at $V_{DS}$ = - 30 V of OFETs at annealing temperatures (a, b) un-annealed (c, d) 120 $^0$C (e, f) 180 $^0$C (g, h) 218 $^0$C. The dashed blue line in (b, d, f and h) represents gate leakage current in the OFETs.

**Table 1.** Electrical parameters of obtained for the LC-OFETs shown in figure 2 at different annealing temperatures of Ph-BTBT-10.

| Annealing temperature ($^0$C) | Saturation Mobility, $\mu_{sat}$ ( $cm^2 V^{-1} s^{-1}$) | $V_{th}$ (V) | $I_{On}$/ $I_{Off}$ |
|---|---|---|---|
| Un-annealed | 5.56 | - 0.87 | 2x $10^4$ |
| 120 | 22.71 | + 0.76 | 6x $10^5$ |
| 180 | 3.41 | - 16.08 | 7x $10^3$ |
| 218 | 0.5 | - 18.20 | 1x $10^3$ |

**Ph-BTBT-10 Layer Characterization.** The electrical characteristics of OFETs show clear dependence on the annealing temperatures of Ph-BTBT-10. Here, we rule out the influence of underlying PDMS layer as the cross-linked PDMS is stable up to ~ 200 $^0$C.[49] To investigate it in detail, a systematic study of the structural and morphological properties of thermally annealed Ph-BTBT-10 was carried out using small angle x-ray scattering (SAXS), x-ray diffraction (XRD) and atomic force microscopy (AFM) techniques. All these experiments were conducted by annealing Ph-BTBT-10 at room temperature, which are either in their thin/ bulk-film form or in powder form according to the requirement of the technique. To conduct SAXS measurement, the Ph-BTBT-10 films were initially coated on glass substrate and annealed at temperatures 120, 180 and 218 $^0$C. The material is then scratched out of the glass into powder form after cooling it down to room temperature. Figure 3 shows the SAXS pattern obtained for Ph-BTBT-10 at different processing temperatures. A comparatively high intensity peak (001), which corresponds to a d-spacing of 5.24 nm, is observed for the samples that are un-annealed, annealed at 120 and 180 $^0$C. This peak represents the typical bilayer structure of the SmE phase of Ph-BTBT-10.[11, 50] Whereas, for the sample annealed at 218 $^{0}$C (temperature corresponding to the SmA phase), only a single peak corresponding to the (002) plane is present. This peak corresponds to a d-spacing of 2.61nm, which is the length of one Ph-BTBT-10 molecule, and so the material has a monolayer structure.[9, 11, 50-51] Hence, it can be concluded that the Ph-BTBT-10 structure has undergone a complete transition from bilayer to monolayer as the temperature is increased above its SmE to SmA phase transition temperature (~ 211 $^{0}$C as per the DSC curve shown in figure S1).[9, 11] Interestingly, even after cooling the sample down to room temperature, the annealed films continued to maintain the structural properties of the SmA and SmE LC phases without undergoing any further reorientation. Furthermore, the sample annealed at 120 $^{0}$C exhibits a high intensity peak corresponding to the (001) plane showing the presence of a bilayer structure. This indicates a strong herringbone packing in it compared to other films.[52] These structural changes in Ph-BTBT-10 as a result of thermal annealing might have affected the electrical performance OFETs as the charge carrier transport occurs through the semiconductor channel.

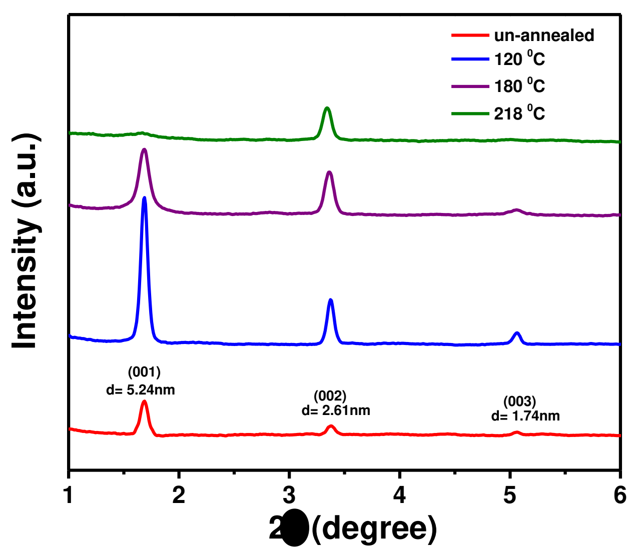


**Figure 3.** SAXS pattern of Ph-BTBT-10 powder annealed at 120, 180 and 218 $^{0}$C.

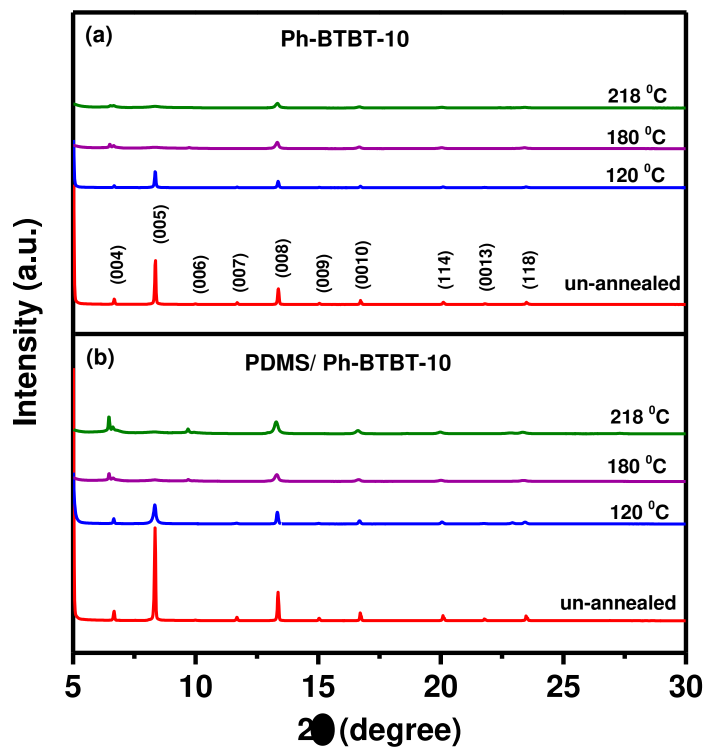


**Figure 4.** XRD pattern of Ph-BTBT-10 films drop-casted on (a) glass surface and (b) PDMS surface that are annealed at temperatures 120, 180 and 218 $^0$C.

The XRD patterns of Ph-BTBT-10 films, drop-casted on glass as well as PDMS are shown in figure 4. The patterns agree with the literature values.[53] The XRD patterns of Ph-BTBT-10 do not show any difference with the change in substrates as seen in figure 4a and 4b. However, the intensity of the peaks seem to increase when coated on PDMS. Noticeable differences are observed among the films annealed at different temperatures. The film annealed at 120 $^0$C and the un-annealed film have similar patterns. However, as the annealing temperature is increased, some of the peaks started disappearing or diminishing as seen in the case of films annealed at 180 and 218

$^{0}$C. Here again, similar to the SAXS pattern, the XRD peaks of films annealed at 120 $^{0}$C show the features of strong crystallinity compared to films annealed at higher temperatures. For example, for the un-annealed film and the film annealed at 120 $^{0}$C, peak corresponding to the (005) plane is prominent whereas, at elevated temperatures these peaks become less prominent.

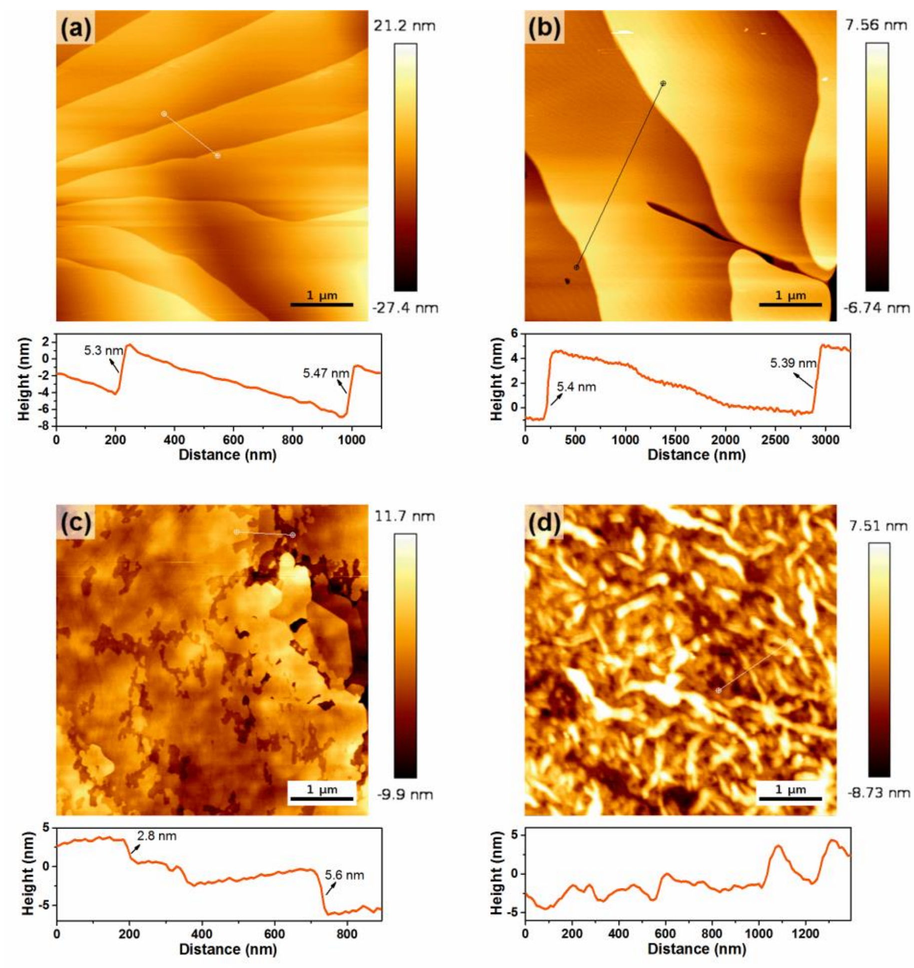


**Figure 5.** AFM images of spin-coated Ph-BTBT-10 thin films on glass surface at different annealing conditions and their corresponding surface profiles: (a) Un-annealed, annealed at (b) 120 $^{0}$C, (c) 180 $^{0}$C and (d) 218 $^{0}$C.

Figure 5 shows the AFM images (5 μm x 5 μm) of Ph- BTBT-10 thin films spin-coated on glass surface and annealed at different temperatures. The films exhibit good material coverage over the substrate surface and possess low surface roughness (Table S3). The un-annealed film contains many well-oriented crystallites with a flake-like structure (figure 5a). A similar flat, terrace-like morphology is observed for the films annealed at 120 $^{0}$C also, but here the grain size is larger (figure 5b) compared to the un-annealed film. From the surface profiling of AFM images of un-annealed films and films annealed at 120 $^{0}$C, over a selected region, it is found that the height of each layer is around 5.6 nm or a multiple of it. This is an indication of the presence of bilayer structure in the films, in accordance with the results obtained from the SAXS pattern. However, as the annealing temperature is increased to 180 $^{0}$C, the grain size is decreased and the film uniformity is lost (figure 5c). Also a random orientation of grains is observed. The films show regions with layer heights of ~2.8 nm and ~ 5.6 nm, which is a clear indication of the presence of both monolayer and bilayer structures.[9] This is again consistent with the SAXS data where the films annealed at 180 $^{0}$C showed peaks of similar intensity corresponding to the d-spacing of 2.61 nm and 5.24 nm. Whereas, when the annealing temperature is raised to 218 $^{0}$C, the film morphology has changed completely and the terrace-like regions are absent in the film. The morphology of the Ph- BTBT-10 thin films on PDMS surface (see supporting information for AFM images (figure S4) and roughness data (Table S4)) is also examined. The results are similar to that obtained on glass substrates, except for the presence of smaller grains with increased surface roughness. The increased surface roughness can be associated with the wrinkled morphological features present on the UVO treated PDMS.[36] Wrinkles (surface with hills and valleys) generally form on the surface of the highly viscoelastic PDMS films when it is subjected to thermal curing like annealing or UVO treatment due to the release of mechanical stress.[31, 36] The surface roughness can also be caused by the evaporation of volatile fragments from the surface of PDMS when the siloxane component gets converted to silicon oxides during UVO treatment.[36]

The variation in OFET characteristics for different annealing temperatures of Ph-BTBT-10 can be correlated to the corresponding change in crystallinity and morphology of Ph-BTBT-10. As the films were casted from a hot solution of Ph-BTBT-10 maintained at a temperature of ~ 110 $^0$C the un-annealed films showed the structural and morphological features of a SmE phase. The SmE phase is characterized by the presence of a few number of monolayers and large number of bilayer structures and this bilayer structure is preserved in the un-annealed film. The SmE phase is known to exhibit closely packed herringbone structure, with a head to head orientation of two molecules at the layer interface forming a bilayer, favoring two-dimensional charge conduction.[9, 11, 53] Hence, the OFET with un-annealed film exhibits good electrical characteristics. However, when the film is annealed at 120 $^0$C, the number of bilayer structures in the sample has increased, as observed from SAXS and AFM measurements, resulting in the exceptionally high performance of corresponding OFETs. Conversely, as the annealing temperature is increased to 180 $^0$C, the monolayer- bilayer intensities have equalized and the OFET performance degraded. A further increase in annealing temperature to 218 $^0$C has resulted in a sudden drop in the OFET performance due to the complete transition of the structure from bilayer to monolayer. Not only the structural properties, but also the variation in grain size (as observed in the AFM images), and the modification in the semiconductor- dielectric interface properties with annealing temperature might have affected the performance of the OFETs. Moreover, the uniform alignment of LCs on PDMS surface has contributed to the ease of charge transport through the LC semiconductor channel. The PDMS surface might have acted as an alignment layer for the Ph-BTBT-10 molecules.[54]

**Influence of Environmental conditions on OFET Performance.** The performance of organic devices are largely dependent on the environment in which it is operated. The fabrication and electrical characterization of the LC-OFETs discussed so far were carried out in ambient conditions. In order to observe its response in other environments, we have done the complete fabrication and electrical characterization of the OFET in nitrogen environment as well. Later, the OFET is taken to air and vacuum conditions. The characteristics obtained for the OFETs with Ph-BTBT-10 film annealed at 120 $^{0}$C at different environments is as shown in figure 6 and the electrical parameters derived are given in table S5. The LC-OFET exhibited a very weak performance in nitrogen environment as compared to the superior performances observed in air as seen in the previous discussions, however non-idealities are not-present. The drain current became low and the off current is increased resulting in a low current on/ off ratio. The OFET showed positive threshold voltage as in a 'normally on' device. The performance of OFET is improved as it is taken into ambient environment (air) as seen in figure 6 (c, d). The mobility, current on/off ratio and threshold voltage showed noticeable enhancement in ambient conditions where the humidity is maintained at ~ 40%. However, the OFET performance is reduced when it is characterized in a vacuum ($10^{-3}$ mbar) condition. Nonetheless, the current on/ off ratio was higher than that obtained when characterized in nitrogen atmosphere. The variation in OFET performance with environmental conditions can occur either due to the changes happening in the semiconductor or in the dielectric. Since we have adopted a BGTC configuration for OFET fabrication, the dielectric layer is placed beneath the semiconductor whereas, the semiconductor is directly exposed to outer environment. Moreover, PDMS is a highly hydrophobic and almost inert material to be effected by environmental changes. As a result, the observed change in electrical characteristics may be attributed to the direct interaction of Ph-BTBT-10 with the environment.

Similar enhancement in hole conductivity is reported for polythiophene (P3HT) material when exposed to air.[55]

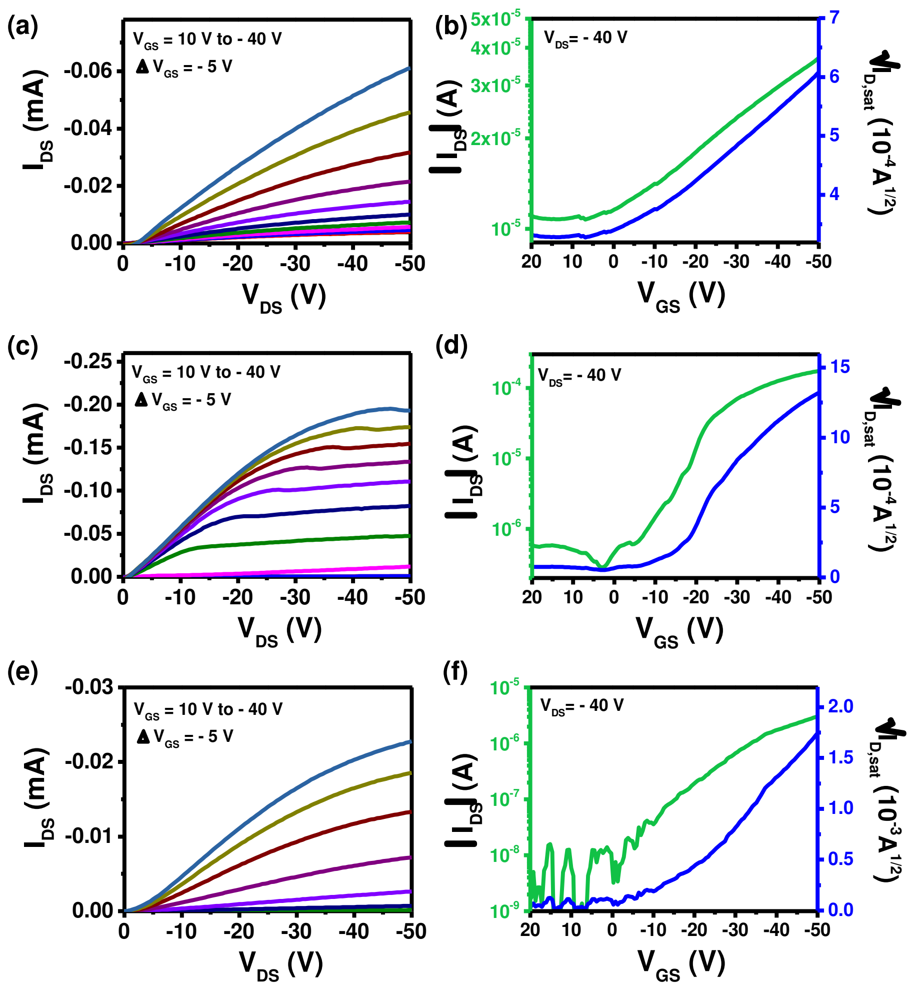


**Figure 6.** (a, c, e) Output characteristics ($I_{DS}$ -$V_{DS}$) and (b, d, f) transfer characteristics ($|I_{DS}|$- $V_{GS}$ and $\sqrt{I_{D,\ sat}}$ -$V_{GS}$) at $V_{DS}$ = - 40 V of the OFET characterized in (a,b) nitrogen (c,d) air and (e,f) vacuum.

**Environmental stability of LC-OFETs.** The stability of the OFETs were analyzed by fabricating and storing the OFETs in air and nitrogen environments for more than three months. Even though the OFET characterized in air exhibited high performance compared to the one characterized in nitrogen atmosphere, the device is found to be more stable in nitrogen than in ambient air. Figure 7 shows the variation in mobility of the OFETs with number of days of storage in air and nitrogen. The device stored in air shows a fast decay in mobility with storage time whereas the decay is slow in the device which is stored in nitrogen. The presence of air is responsible for an initial shoot-up in the mobility, however the storage in air causes a decay in performance due to the interaction of the organic components with water molecules and other impurities in air causing the creation of trap states and defects in the organic layers over time. The exact reason of enhanced performance and stability issue in air needs a detailed study which is beyond the scope of the present work.

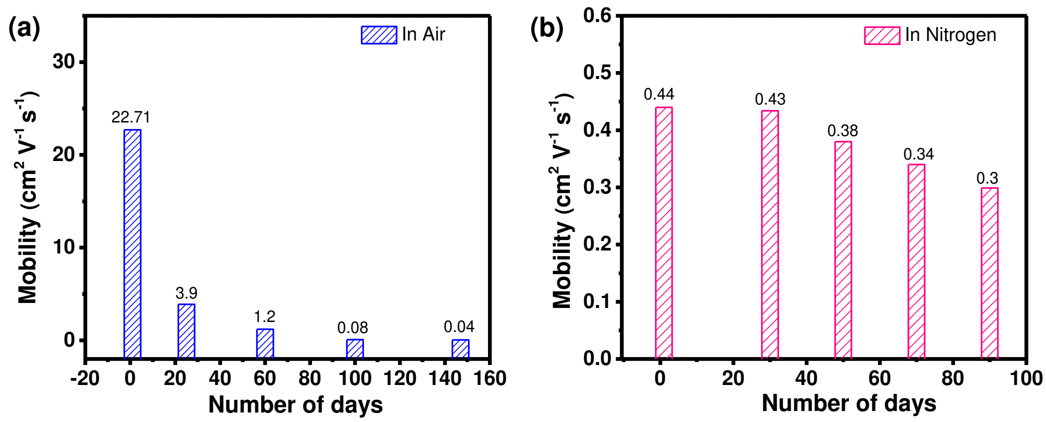


**Figure 7.** Variation in field effect mobility with number of days of storage (a) in air and (b) in nitrogen.

**Electrical Stability and hysteresis of PDMS based LC-OFETs.** The electrical stability of LC-OFET which is fabricated by annealing Ph-BTBT-10 layer at 120 $^0$C is studied by conducting bias-stress measurements in air. The drain and gate voltages (fixed at -20 V each) were continuously applied for 5000 s and observed the variation in drain current with time. Unlike the exponential decay normally observed in OFETs due to the presence of trap states, the LC-OFET in the present study exhibited anomalous current transients (figure 8a). Here, instead of a decay, the drain current showed an abrupt initial rise followed by a slow decay. The abrupt initial increase of $I_{DS}$ can be mainly due to the slow-polarization of PDMS (due to its low dielectric constant). It can also occur due to the presence of dipolar groups on PDMS surface or due to the gate charge injection.[56-57] We also observed similar rise of current in nitrogen and vacuum also but the rate of increase is much smaller compared to that in air. Similarly, in humid conditions, a fast decay is observed which supports the fast decay in mobility shown by LC-OFET when stored in air. The fluctuations in ambient air and moisture show large influence on the LC-OFET performance. The bias-stress measurements indicate the high electrical stability of LC-OFETs against a continuous bias-stress.

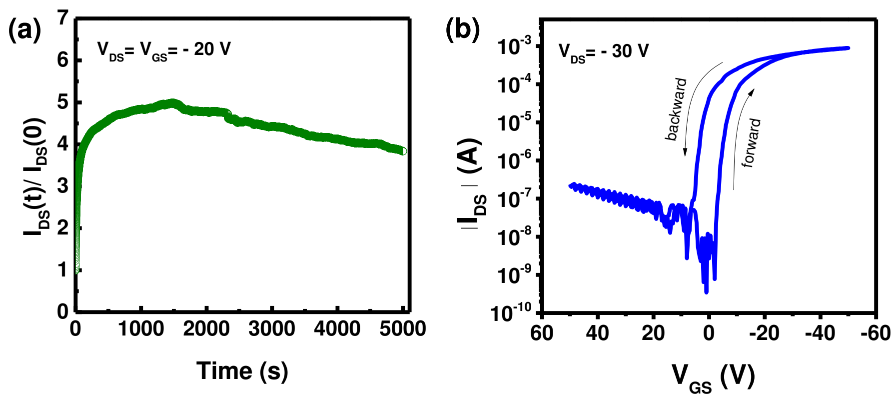


**Figure 8.** (a) The normalized drain current versus time relation under the application of a continuous bias-stress ($V_{DS}$= $V_{GS}$= - 20 V) for 5000 s and (b) the transfer characteristics showing hysteresis for the LC-OFET with Ph-BTBT-10 layer annealed at 120 $^0$C when characterized in air.

As shown in figure 8b, the LC-OFETs exhibit hysteresis behavior with a lower drain current during forward sweep (off to on) and a higher drain current during the backward sweep (on to off). This kind of hysteresis can occur due to the same reasons that causes anomalous bias-stress behavior, which includes slow-polarization of PDMS and presence of polar functional groups on the gate dielectric.[58] As in the case of bias-stress, hysteresis is also found to be dependent on atmospheric conditions and is more pronounced in air than in nitrogen atmosphere. A detailed investigation on the bias-stress and hysteresis behavior of PDMS based OFETs and the role of semiconductors, atmospheric factors in it is being conducted. Suitable remedy for hysteresis nature is to be identified which may also reduce non-ideal behavior of the device.

## CONCLUSION

In summary, the high performance of LC-OFETs with the LC, Ph- BTBT-10 as channel material and the polymer elastomer, PDMS as gate dielectric is demonstrated. The devices exhibit high performances such as high hole mobility of ~ 22 $cm^2V^{-1}s^{-1}$, low threshold voltage (< 1 V) and high current on/ off ratio of $10^5$, irrespective of the low dielectric constant of PDMS. The possibility of overestimation in mobility values due to the non-ideal transistor behavior was taken into account during mobility calculation. The annealing temperature of the LC is found to have large influence on the performance of the LC- OFETs. The OFET with Ph-BTBT-10 film annealed at 120 $^0$C exhibits superior performance than the devices fabricated with un-annealed film and with the films annealed at 180 and 218 $^0$C. The enhanced performance is attributed to many factors like the bilayer structure and the large grain size of Ph-BTBT-10, and good dielectric-semiconductor interface properties. Moreover, the PDMS layer has acted as a proper alignment layer for the LC molecules, ensuring high carrier mobility for the OFETs through the channel. The LC-OFETs are found to be influenced by the environmental conditions in which it is operated, such as in air, nitrogen and vacuum conditions. The OFETs show anomalous bias-stress behavior and hysteresis, however, they are electrically stable. The transparent solution-processed LC-OFET is a promising prototype for flexible electronics.

## ASSOCIATED CONTENT

**Supporting Information**. (1) UVO treatment mechanism on PDMS surface, (2) primary characterization methods of Ph-BTBT-10: optical image of Ph-BTBT-10 thin-film, DSC curve, POM images of the phases of PhBTBT-10, (3) Capacitance- Frequency characteristics of PDMS, (4) table containing reliability factors of mobility, (5) table with average mobility of OFETs, (6) Mobility versus Annealing temperature plot, (7) Table containing the surface roughness of Ph-BTBT-10 thin-films, (8) AFM images of Ph-BTBT-10 on PDMS surface, (9) Table containing surface roughness of Ph-BTBT-10 thin-films on PDMS, (10) table containing electrical parameters of LC-OFET characterized at air, nitrogen and vacuum environments, (11) transfer characteristics showing hysteresis, (12) nature of hysteresis in air and nitrogen. (single PDF)

## AUTHOR INFORMATION

### Corresponding Author

**Manoj A. G. Namboothiry**

School of Physics, Indian Institute of Science Education and Research- Thiruvananthapuram, Maruthamala P O, Vithura, Thiruvananthapuram, Kerala- 695551, India

ORCID: 0000-0002-7805-1962

E-mail: manoj@iisertvm.ac.in

**Authors**

**Reshma Raveendran**

School of Physics, Indian Institute of Science Education and Research- Thiruvananthapuram, Maruthamala P O, Vithura, Thiruvananthapuram, Kerala- 695551, India

ORCID: 0000-0003-0866-3039

**Mamatha Nagaraj**

School of Physics and Astronomy, University of Leeds, Leeds LS2 9JT, UK

ORCID: 0000-0001-9713-1362

E-mail: m.nagaraj@leeds.ac.uk

**Author Contributions**

The manuscript was written through contributions of all authors. All authors have given approval to the final version of the manuscript.

**Notes**

The authors declare no competing financial interest.

## ACKNOWLEDGMENTS

This work is supported by the Solar Energy Research Initiative (Department of Science and Technology, Government of India) and the Ministry of Human Resource and Development (Government of India). R.R. wishes to thank the Department of Science and Technology for the INSPIRE fellowship and the Newton- Bhabha short-term PhD placement program 2019 (jointly funded by British Council, UK and DST, India). M.A.G.N. and R.R. acknowledge Dr.

Ayyappanpillai Ajayaghosh and Dr. Bhoje E. Gowd, CSIR-National Institute for Interdisciplinary Science and Technology, Thiruvananthapuram for SAXS measurements.

## REFERENCES

(1) Sirringhaus, H. 25th Anniversary Article: Organic Field-Effect Transistors: The Path Beyond Amorphous Silicon. *Advanced Materials* **2014,** *26* (9), 1319-1335, DOI: 10.1002/adma.201304346.

(2) Yuan, Y.; Giri, G.; Ayzner, A. L.; Zoombelt, A. P.; Mannsfeld, S. C. B.; Chen, J.; Nordlund, D.; Toney, M. F.; Huang, J.; Bao, Z. Ultra-high mobility transparent organic thin film transistors grown by an off-centre spin-coating method. *Nature Communications* **2014,** *5* (1), 3005, DOI: 10.1038/ncomms4005.

(3) Pei, K.; Wang, Z.; Ren, X.; Zhang, Z.; Peng, B.; Chan, P. K. L. Fully transparent organic transistors with junction-free metallic network electrodes. *Appl. Phys. Lett.* **2015,** *107* (3), 033302, DOI: 10.1063/1.4927445.

(4) Lee, S.; Reuveny, A.; Reeder, J.; Lee, S.; Jin, H.; Liu, Q.; Yokota, T.; Sekitani, T.; Isoyama, T.; Abe, Y.; Suo, Z.; Someya, T. A transparent bending-insensitive pressure sensor. *Nature Nanotechnology* **2016,** *11* (5), 472-478, DOI: 10.1038/nnano.2015.324.

(5) Liang, J.; Li, L.; Chen, D.; Hajagos, T.; Ren, Z.; Chou, S.-Y.; Hu, W.; Pei, Q. Intrinsically stretchable and transparent thin-film transistors based on printable silver nanowires, carbon nanotubes and an elastomeric dielectric. *Nature Communications* **2015,** *6* (1), 7647, DOI: 10.1038/ncomms8647.

(6) Halik, M.; Klauk, H.; Zschieschang, U.; Schmid, G.; Radlik, W.; Weber, W. Polymer Gate Dielectrics and Conducting-Polymer Contactsfor High-Performance Organic Thin-Film Transistors. *Advanced Materials* **2002,** *14* (23), 1717-1722, DOI: 10.1002/1521-4095(20021203)14:23<1717::aid-adma1717>3.0.co;2-g.

(7) Veres, J.; Ogier, S.; Lloyd, G.; de Leeuw, D. Gate Insulators in Organic Field-Effect Transistors. *Chemistry of Materials* **2004,** *16* (23), 4543-4555, DOI: 10.1021/cm049598q.

(8) Nketia-Yawson, B.; Noh, Y.-Y. Recent Progress on High-Capacitance Polymer Gate Dielectrics for Flexible Low-Voltage Transistors. *Advanced Functional Materials* **2018,** *28* (42), 1802201, DOI: 10.1002/adfm.201802201.

(9) Iino, H.; Usui, T.; Hanna, J.-i. Liquid crystals for organic thin-film transistors. *Nature Communications* **2015,** *6* (1), 6828, DOI: 10.1038/ncomms7828.

(10) Kunii, M.; Iino, H.; Hanna, J. Solution-Processed, Low-Voltage Polycrystalline Organic Field-Effect Transistor Fabricated Using Highly Ordered Liquid Crystal With Low- $k$ Gate Dielectric. *IEEE Electron Device Letters* **2016,** *37* (4), 486-488, DOI: 10.1109/LED.2016.2529678.

(11) Kim, S.; Kim, A.; Jang, K.-S.; Yoo, S.; Ka, J.-W.; Kim, J.; Yi, M. H.; Won, J. C.; Hong, S.-K.; Kim, Y. H. The effect of thermal annealing on the layered structure of smectic liquid crystalline organic semiconductor on polyimide gate insulator and its OFET performance. *Synthetic Metals* **2016,** *220*, 311-317, DOI: https://doi.org/10.1016/j.synthmet.2016.06.021.

(12) Wang, Y.; Huang, X.; Li, T.; Li, L.; Guo, X.; Jiang, P. Polymer-Based Gate Dielectrics for Organic Field-Effect Transistors. *Chemistry of Materials* **2019,** *31* (7), 2212-2240, DOI: 10.1021/acs.chemmater.8b03904.
(13) He, D.; Qiao, J.; Zhang, L.; Wang, J.; Lan, T.; Qian, J.; Li, Y.; Shi, Y.; Chai, Y.; Lan, W.; Ono, L. K.; Qi, Y.; Xu, J.-B.; Ji, W.; Wang, X. Ultrahigh mobility and efficient charge injection in monolayer organic thin-film transistors on boron nitride. *Science Advances* **2017,** *3* (9), e1701186, DOI: 10.1126/sciadv.1701186.
(14) Lee, J.; Kang, S.-H.; Lee, S. M.; Lee, K. C.; Yang, H.; Cho, Y.; Han, D.; Li, Y.; Lee, B. H.; Yang, C. An Ultrahigh Mobility in Isomorphic Fluorobenzo[c][1,2,5]thiadiazole-Based Polymers. *Angewandte Chemie International Edition* **2018,** *57* (41), 13629-13634, DOI: 10.1002/anie.201808098.
(15) Lee, B. H.; Hsu, B. B. Y.; Patel, S. N.; Labram, J.; Luo, C.; Bazan, G. C.; Heeger, A. J. Flexible Organic Transistors with Controlled Nanomorphology. *Nano Letters* **2016,** *16* (1), 314-319, DOI: 10.1021/acs.nanolett.5b03868.
(16) Li, J.; Zhao, Y.; Tan, H. S.; Guo, Y.; Di, C.-A.; Yu, G.; Liu, Y.; Lin, M.; Lim, S. H.; Zhou, Y.; Su, H.; Ong, B. S. A stable solution-processed polymer semiconductor with record high-mobility for printed transistors. *Scientific Reports* **2012,** *2* (1), 754, DOI: 10.1038/srep00754.
(17) Tseng, H.-R.; Phan, H.; Luo, C.; Wang, M.; Perez, L. A.; Patel, S. N.; Ying, L.; Kramer, E. J.; Nguyen, T.-Q.; Bazan, G. C.; Heeger, A. J. High-Mobility Field-Effect Transistors Fabricated with Macroscopic Aligned Semiconducting Polymers. *Advanced Materials* **2014,** *26* (19), 2993-2998, DOI: 10.1002/adma.201305084.
(18) Wang, Q.; Jiang, S.; Qian, J.; Song, L.; Zhang, L.; Zhang, Y.; Zhang, Y.; Wang, Y.; Wang, X.; Shi, Y.; Zheng, Y.; Li, Y. Low-voltage, High-performance Organic Field-Effect Transistors Based on 2D Crystalline Molecular Semiconductors. *Scientific Reports* **2017,** *7* (1), 7830, DOI: 10.1038/s41598-017-08280-8.
(19) Xu, X.; Yao, Y.; Shan, B.; Gu, X.; Liu, D.; Liu, J.; Xu, J.; Zhao, N.; Hu, W.; Miao, Q. Electron Mobility Exceeding 10 cm2 V−1 s−1 and Band-Like Charge Transport in Solution-Processed n-Channel Organic Thin-Film Transistors. *Advanced Materials* **2016,** *28* (26), 5276-5283, DOI: 10.1002/adma.201601171.
(20) Piliego, C.; Jarzab, D.; Gigli, G.; Chen, Z.; Facchetti, A.; Loi, M. A. High Electron Mobility and Ambient Stability in Solution-Processed Perylene-Based Organic Field-Effect Transistors. *Advanced Materials* **2009,** *21* (16), 1573-1576, DOI: 10.1002/adma.200803207.
(21) Tang, W.; Feng, L.; Yu, P.; Zhao, J.; Guo, X. Highly Efficient All-Solution-Processed Low-Voltage Organic Transistor with a Micrometer-Thick Low-k Polymer Gate Dielectric Layer. *Advanced Electronic Materials* **2016,** *2* (5), 1500454, DOI: 10.1002/aelm.201500454.
(22) Zhao, J.; Tang, W.; Li, Q.; Liu, W.; Guo, X. Fully Solution Processed Bottom-Gate Organic Field-Effect Transistor With Steep Subthreshold Swing Approaching the Theoretical Limit. *IEEE Electron Device Letters* **2017,** *38* (10), 1465-1468.
(23) Shin, E.-Y.; Choi, E.-Y.; Noh, Y.-Y. Parylene based bilayer flexible gate dielectric layer for top-gated organic field-effect transistors. *Organic Electronics* **2017,** *46*, 14-21, DOI: https://doi.org/10.1016/j.orgel.2017.04.005.
(24) Wang, B.; Huang, W.; Chi, L.; Al-Hashimi, M.; Marks, T. J.; Facchetti, A. High-k Gate Dielectrics for Emerging Flexible and Stretchable Electronics. *Chem. Rev.* **2018,** *118* (11), 5690-5754, DOI: 10.1021/acs.chemrev.8b00045.

(25) Park, H.; Yoo, S.; Yi, M. H.; Kim, Y. H.; Jung, S. Flexible and stable organic field-effect transistors using low-temperature solution-processed polyimide gate dielectrics. *Organic Electronics* **2019,** *68*, 70-75, DOI: https://doi.org/10.1016/j.orgel.2019.01.043.
(26) Facchetti, A.; Yoon, M.-H.; Marks, T. J. Gate Dielectrics for Organic Field-Effect Transistors: New Opportunities for Organic Electronics. *Advanced Materials* **2005,** *17* (14), 1705-1725, DOI: 10.1002/adma.200500517.
(27) Veres, J.; Ogier, S. D.; Leeming, S. W.; Cupertino, D. C.; Mohialdin Khaffaf, S. Low-k Insulators as the Choice of Dielectrics in Organic Field-Effect Transistors. *Advanced Functional Materials* **2003,** *13* (3), 199-204, DOI: 10.1002/adfm.200390030.
(28) Lee, J.; Chung, J. W.; Yoon, G. B.; Lee, M. H.; Kim, D. H.; Park, J.; Lee, J.-K.; Kang, M. S. Influence of Dielectric Layers on Charge Transport through Diketopyrrolopyrrole-Containing Polymer Films: Dielectric Polarizability vs Capacitance. *ACS Applied Materials & Interfaces* **2016,** *8* (44), 30344-30350, DOI: 10.1021/acsami.6b09993.
(29) Lee, S.-H.; Xu, Y.; Khim, D.; Park, W.-T.; Kim, D.-Y.; Noh, Y.-Y. Effect of Polymer Gate Dielectrics on Charge Transport in Carbon Nanotube Network Transistors: Low-k Insulator for Favorable Active Interface. *ACS Applied Materials & Interfaces* **2016,** *8* (47), 32421-32431, DOI: 10.1021/acsami.6b06882.
(30) Reese, C.; Chung, W.-J.; Ling, M.-m.; Roberts, M.; Bao, Z. High-performance microscale single-crystal transistors by lithography on an elastomer dielectric. *Appl. Phys. Lett.* **2006,** *89* (20), 202108, DOI: 10.1063/1.2388151.
(31) Graz, I. M.; Lacour, S. P. Flexible pentacene organic thin film transistor circuits fabricated directly onto elastic silicone membranes. *Appl. Phys. Lett.* **2009,** *95* (24), 243305, DOI: 10.1063/1.3265737.
(32) Orgiu, E.; Manunza, I.; Sanna, M.; Cosseddu, P.; Bonfiglio, A. Transparent dielectric films for organic thin-film transistors: A perspective for low cost, low size technologies. *Thin Solid Films* **2008,** *516* (7), 1533-1537, DOI: https://doi.org/10.1016/j.tsf.2007.03.157.
(33) Zhou, S.; Li, M.; Tang, Q.; Song, Z.; Tong, Y.; Liu, Y. Deposition of Pentacene Thin Film on Polydimethylsiloxane Elastic Dielectric Layer for Flexible Thin-Film Transistors. *IEEE Electron Device Letters* **2017,** *38* (8), 1031-1034.
(34) McDonald, J. C.; Whitesides, G. M. Poly(dimethylsiloxane) as a Material for Fabricating Microfluidic Devices. *Acc. Chem. Res.* **2002,** *35* (7), 491-499, DOI: 10.1021/ar010110q.
(35) Law, K.-Y.; Zhao, H. *Surface wetting: characterization, contact angle, and fundamentals*, Springer 2015.
(36) Raveendran, R.; Namboothiry, M. A. G. Surface-Treated Poly(dimethylsiloxane) as a Gate Dielectric in Solution-Processed Organic Field-Effect Transistors. *ACS Omega* **2018,** *3* (9), 11278-11285, DOI: 10.1021/acsomega.8b01629.
(37) Yamamura, A.; Sakon, T.; Takahira, K.; Wakimoto, T.; Sasaki, M.; Okamoto, T.; Watanabe, S.; Takeya, J. High-Speed Organic Single-Crystal Transistor Responding to Very High Frequency Band. *Advanced Functional Materials* **2020,** *30* (11), 1909501, DOI: 10.1002/adfm.201909501.
(38) Guo, X.; Balon, F.; Hatton, R. A.; Shannon, J. M. In *High Performance Transistors in Low Mobility Organic Semiconductors for Analog and High-Frequency Applications*, 2008 Flexible Electronics and Displays Conference and Exhibition, 21-24 Jan. 2008; 2008; pp 1-5.
(39) Quinn, J. T. E.; Zhu, J.; Li, X.; Wang, J.; Li, Y. Recent progress in the development of n-type organic semiconductors for organic field effect transistors. *Journal of Materials Chemistry C* **2017,** *5* (34), 8654-8681, DOI: 10.1039/C7TC01680H.

(40) McCulloch, I.; Heeney, M.; Bailey, C.; Genevicius, K.; MacDonald, I.; Shkunov, M.; Sparrowe, D.; Tierney, S.; Wagner, R.; Zhang, W.; Chabinyc, M. L.; Kline, R. J.; McGehee, M. D.; Toney, M. F. Liquid-crystalline semiconducting polymers with high charge-carrier mobility. *Nature Materials* **2006,** *5* (4), 328-333, DOI: 10.1038/nmat1612.
(41) Funahashi, M. Development of Liquid-Crystalline Semiconductors with High Carrier Mobilities and Their Application to Thin-film Transistors. *Polymer Journal* **2009,** *41* (6), 459-469, DOI: 10.1295/polymj.PJ2008324.
(42) Choi, H. H.; Cho, K.; Frisbie, C. D.; Sirringhaus, H.; Podzorov, V. Critical assessment of charge mobility extraction in FETs. *Nature Materials* **2018,** *17* (1), 2-7, DOI: 10.1038/nmat5035.
(43) Gundlach, D. J.; Zhou, L.; Nichols, J. A.; Jackson, T. N.; Necliudov, P. V.; Shur, M. S. An experimental study of contact effects in organic thin film transistors. *J. Appl. Phys.* **2006,** *100* (2), 024509, DOI: 10.1063/1.2215132.
(44) Phan, H.; Ford, M. J.; Lill, A. T.; Wang, M.; Bazan, G. C.; Nguyen, T.-Q. Electrical Double-Slope Nonideality in Organic Field-Effect Transistors. *Advanced Functional Materials* **2018,** *28* (17), 1707221, DOI: 10.1002/adfm.201707221.
(45) Park, S.; Lee, B.; Bae, B.; Chai, J.; Lee, S.; Kim, C. Ambipolar thin-film transistors based on organic semiconductor blend. *Synthetic Metals* **2019,** *253*, 40-47, DOI: https://doi.org/10.1016/j.synthmet.2019.05.001.
(46) Bittle, E. G.; Basham, J. I.; Jackson, T. N.; Jurchescu, O. D.; Gundlach, D. J. Mobility overestimation due to gated contacts in organic field-effect transistors. *Nature Communications* **2016,** *7* (1), 10908, DOI: 10.1038/ncomms10908.
(47) Paterson, A. F.; Singh, S.; Fallon, K. J.; Hodsden, T.; Han, Y.; Schroeder, B. C.; Bronstein, H.; Heeney, M.; McCulloch, I.; Anthopoulos, T. D. Recent Progress in High-Mobility Organic Transistors: A Reality Check. *Advanced Materials* **2018,** *30* (36), 1801079, DOI: 10.1002/adma.201801079.
(48) Un, H.-I.; Wang, J.-Y.; Pei, J. Recent Efforts in Understanding and Improving the Nonideal Behaviors of Organic Field-Effect Transistors. *Advanced Science* **2019,** *6* (20), 1900375, DOI: 10.1002/advs.201900375.
(49) Liu, M.; Sun, J.; Chen, Q. Influences of heating temperature on mechanical properties of polydimethylsiloxane. *Sensors and Actuators A: Physical* **2009,** *151* (1), 42-45, DOI: https://doi.org/10.1016/j.sna.2009.02.016.
(50) Inoue, S.; Minemawari, H.; Tsutsumi, J. y.; Chikamatsu, M.; Yamada, T.; Horiuchi, S.; Tanaka, M.; Kumai, R.; Yoneya, M.; Hasegawa, T. Effects of Substituted Alkyl Chain Length on Solution-Processable Layered Organic Semiconductor Crystals. *Chemistry of Materials* **2015,** *27* (11), 3809-3812, DOI: 10.1021/acs.chemmater.5b00810.
(51) Iino, H.; Hanna, J.-I. Liquid crystal and crystal structures of a phenyl-benzothienobenzothiophene derivative. *Mol. Cryst. Liq. Cryst.* **2017,** *647* (1), 37-43, DOI: 10.1080/15421406.2017.1289427.
(52) Cullity, B. D. Elements of X-ray diffraction, Addison. *Wesley Mass* **1978**.
(53) Minemawari, H.; Tsutsumi, J. y.; Inoue, S.; Yamada, T.; Kumai, R.; Hasegawa, T. Crystal structure of asymmetric organic semiconductor 7-decyl-2-phenyl[1]benzothieno[3,2-b][1]benzothiophene. *Applied Physics Express* **2014,** *7* (9), 091601, DOI: 10.7567/apex.7.091601.
(54) Sun, X.; Di, C.-a.; Liu, Y. Engineering of the dielectric–semiconductor interface in organic field-effect transistors. *Journal of Materials Chemistry* **2010,** *20* (13), 2599-2611, DOI: 10.1039/B921449F.

(55) Abdou, M. S. A.; Orfino, F. P.; Son, Y.; Holdcroft, S. Interaction of Oxygen with Conjugated Polymers: Charge Transfer Complex Formation with Poly(3-alkylthiophenes). *J. Am. Chem. Soc.* **1997,** *119* (19), 4518-4524, DOI: 10.1021/ja964229j.
(56) Kim, J.; Jang, J.; Kim, K.; Kim, H.; Kim, S. H.; Park, C. E. The Origin of Excellent Gate-Bias Stress Stability in Organic Field-Effect Transistors Employing Fluorinated-Polymer Gate Dielectrics. *Advanced Materials* **2014,** *26* (42), 7241-7246, DOI: 10.1002/adma.201402363.
(57) de Pauli, M.; Zschieschang, U.; Barcelos, I. D.; Klauk, H.; Malachias, A. Tailoring the Dielectric Layer Structure for Enhanced Carrier Mobility in Organic Transistors: The Use of Hybrid Inorganic/Organic Multilayer Dielectrics. *Advanced Electronic Materials* **2016,** *2* (5), 1500402, DOI: 10.1002/aelm.201500402.
(58) Egginger, M.; Bauer, S.; Schwödiauer, R.; Neugebauer, H.; Sariciftci, N. S. Current versus gate voltage hysteresis in organic field effect transistors. *Monatsh. Chem.* **2009,** *140*, 735-750, DOI: 10.1007/s00706-009-0149-z.

For Table of Contents Only

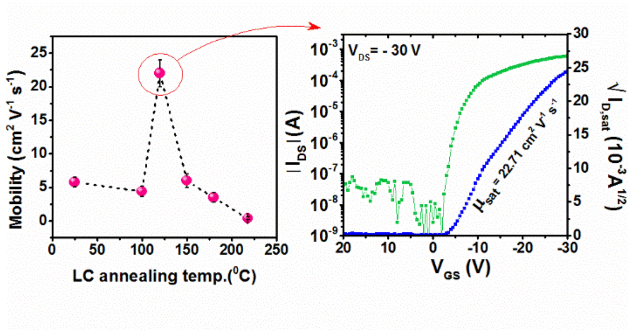

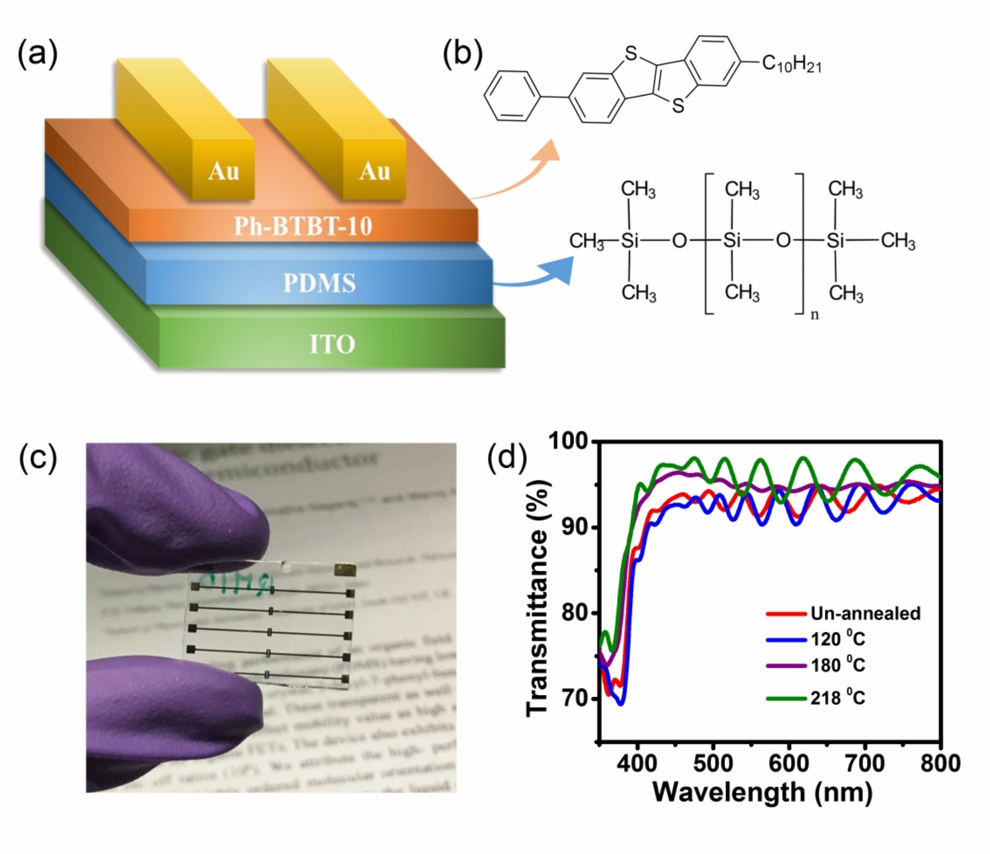


152x131mm (600 x 600 DPI)

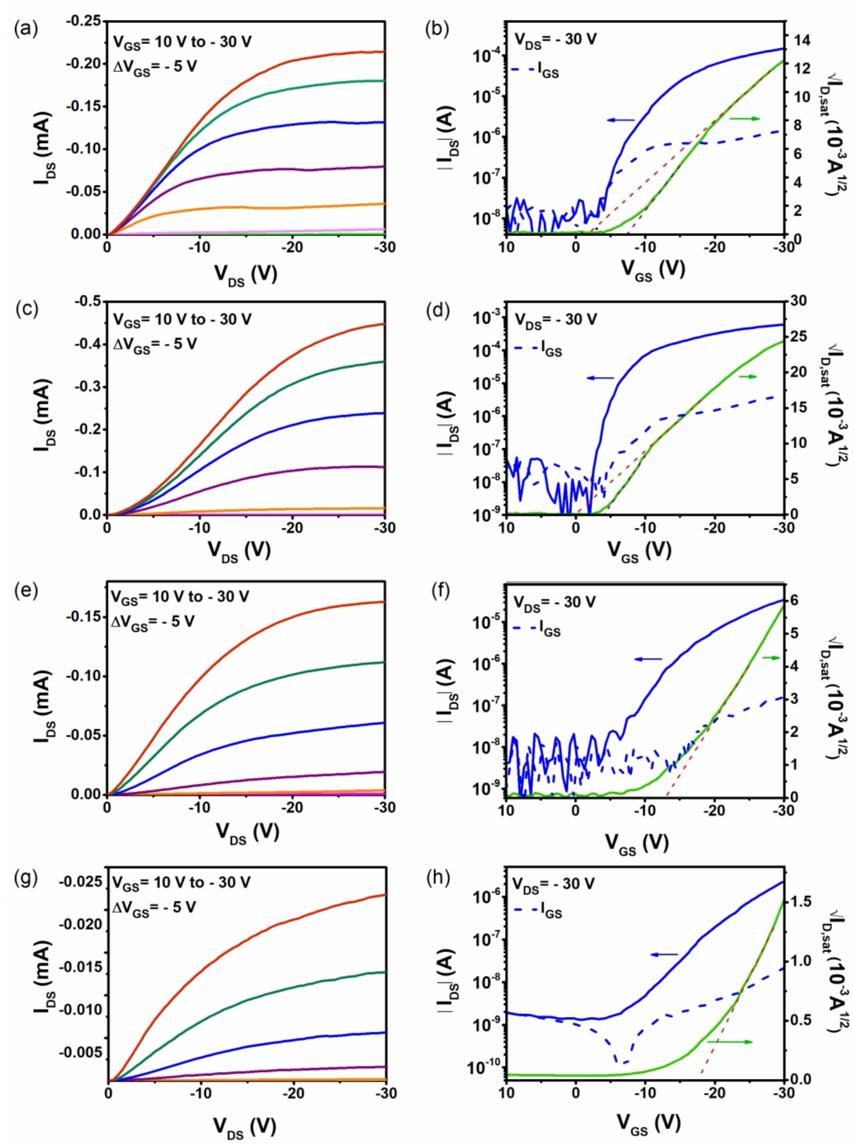


211x295mm (300 x 300 DPI)

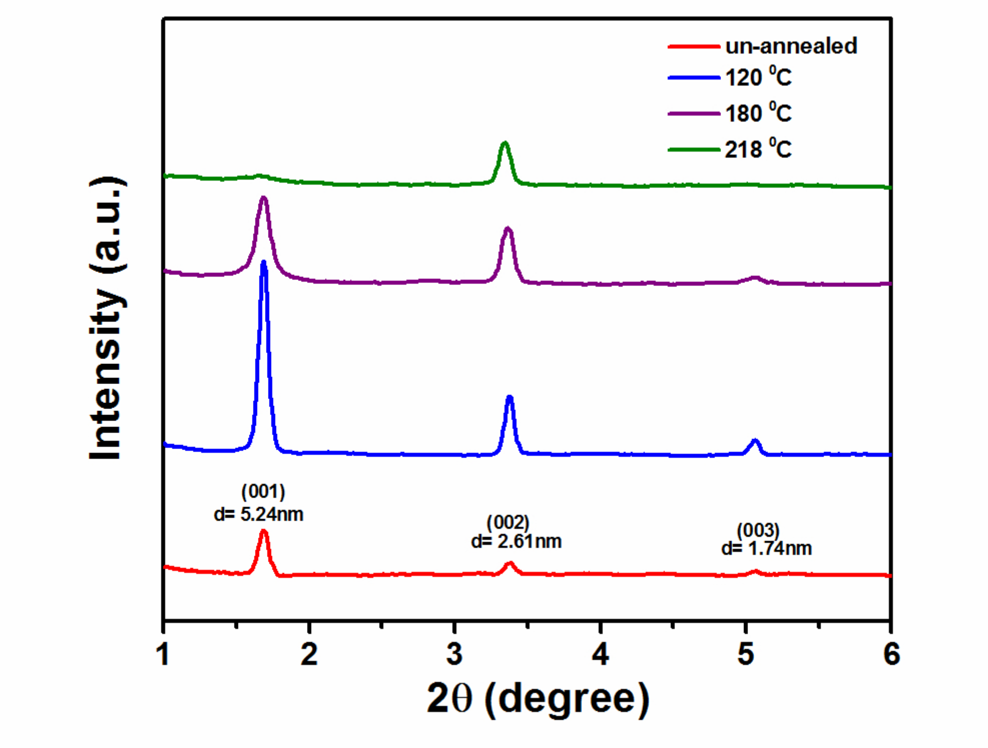


84x64mm (300 x 300 DPI)

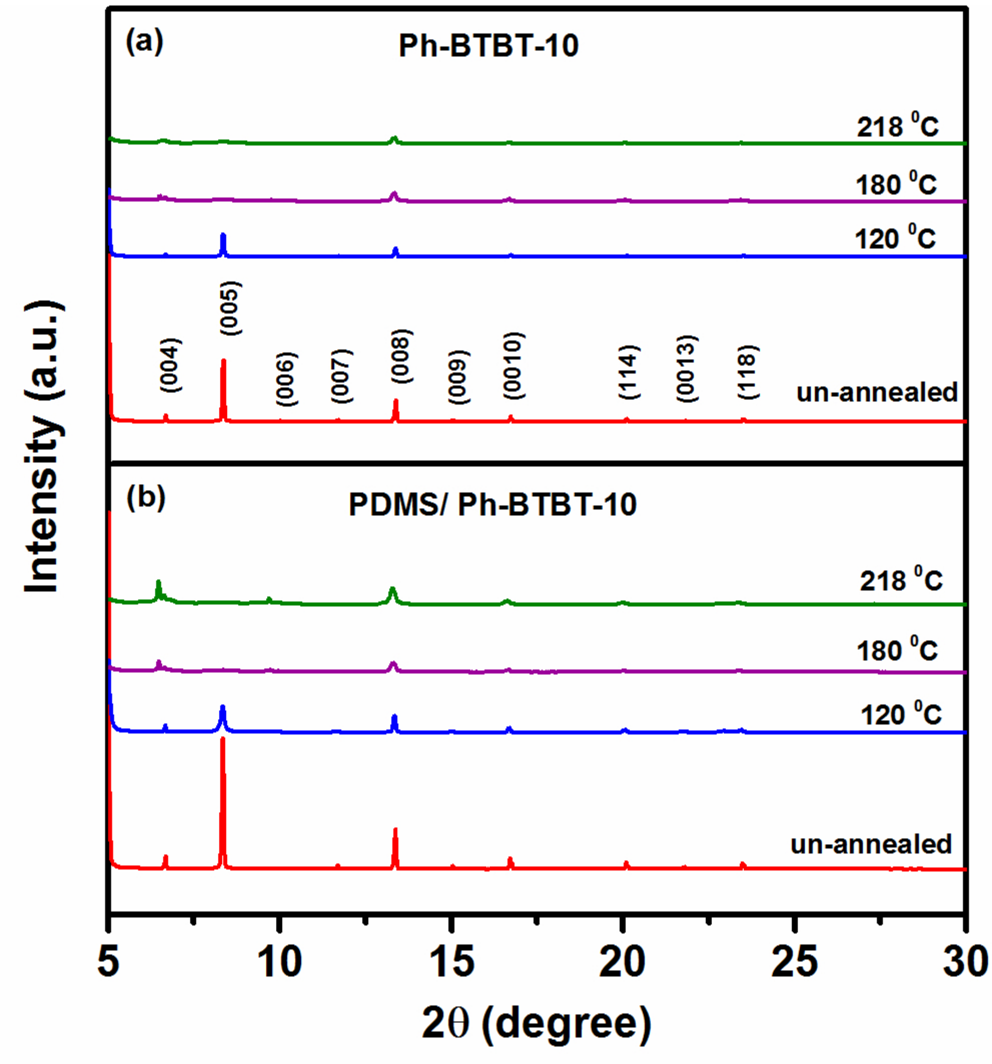


84x90mm (300 x 300 DPI)

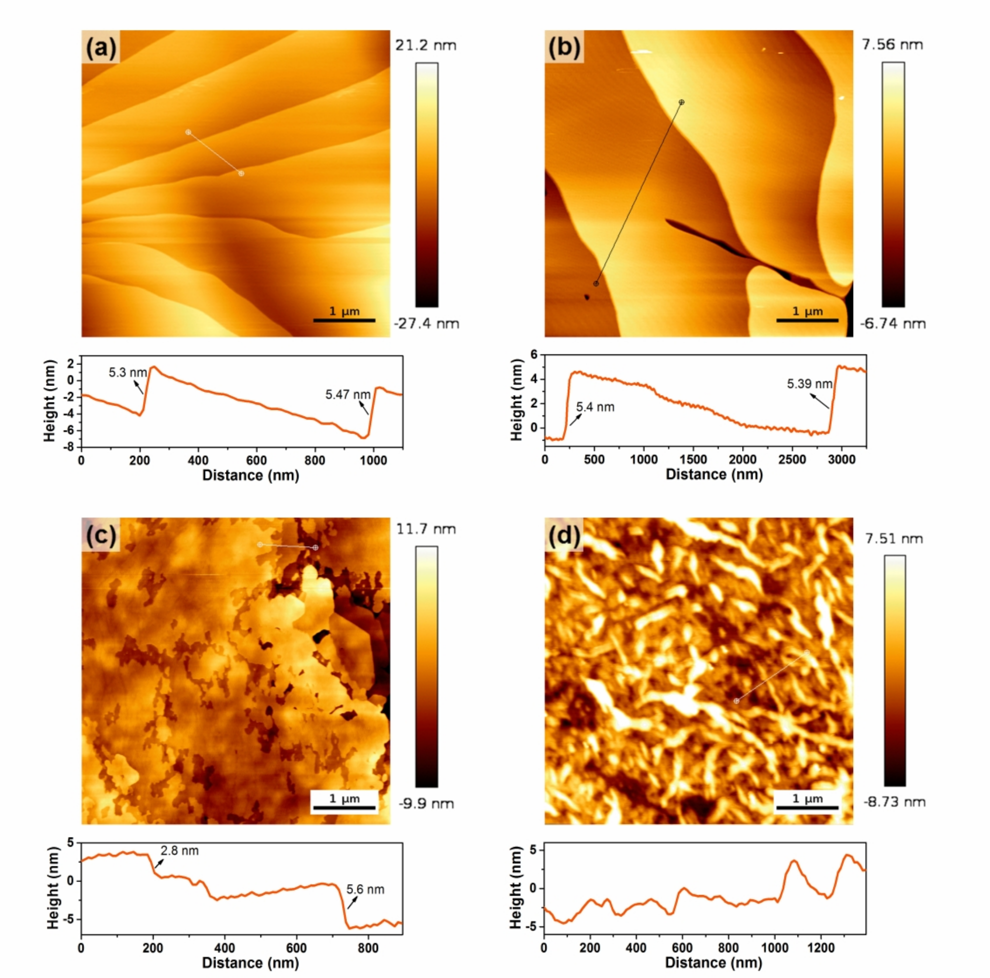


177x176mm (600 x 600 DPI)

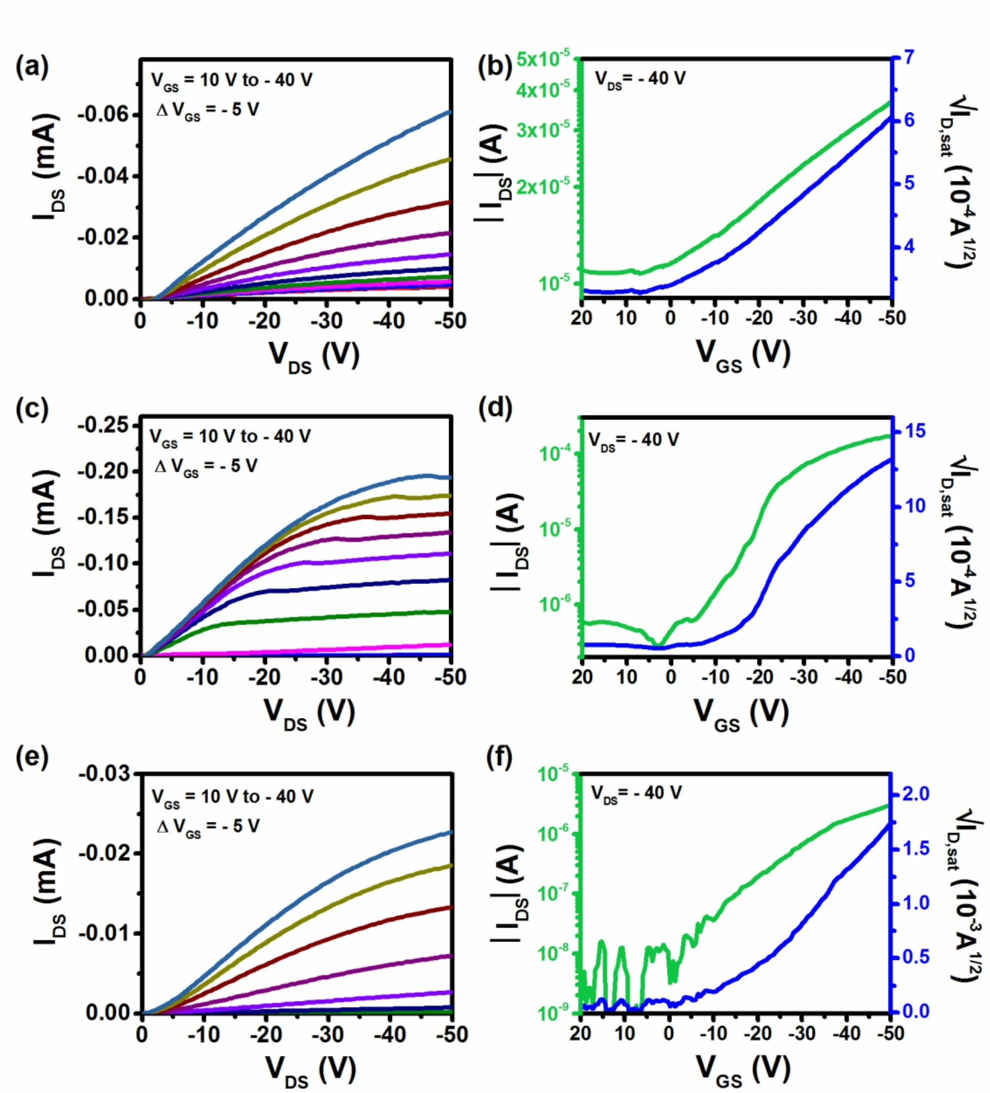


152x169mm (300 x 300 DPI)

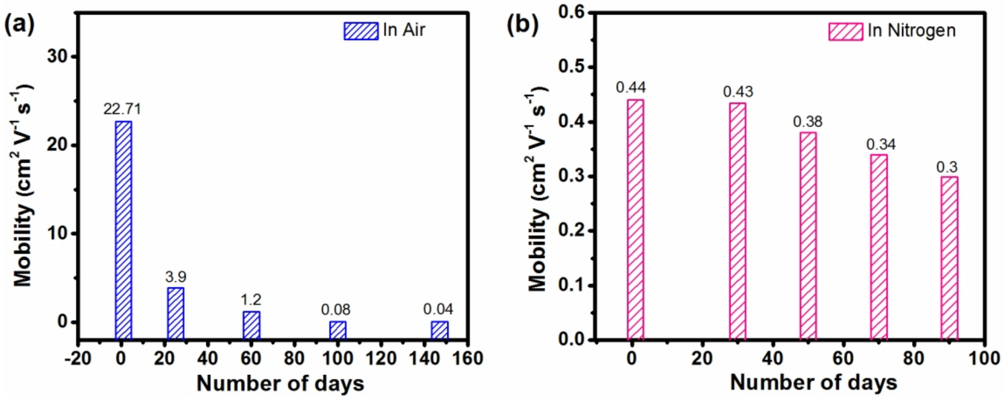


152x61mm (300 x 300 DPI)

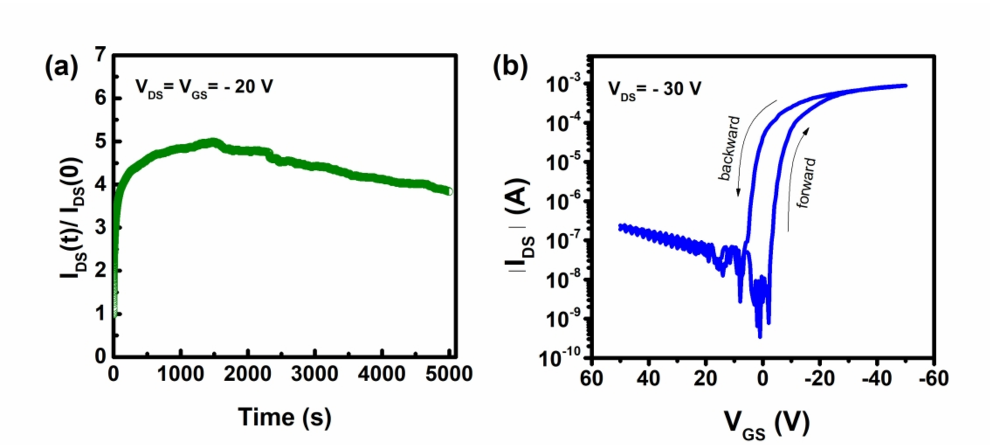


273x122mm (300 x 300 DPI)